Proposal of a multi-standard transceiver for the WBAN Internet of Things

Jianxiao Yang, Benoit Geller, Tarak Arbi

HAL Id: hal-01626262
https://ensta-paris.hal.science/hal-01626262

PROPOSAL OF A MULTI-STANDARD TRANSCEIVER FOR THE WBAN INTERNET OF THINGS

Jianxiao Yang, Benoit Geller, Tarak Arbi

Department U2IS, ENSTA-ParisTech, Palaiseau, France
jianxiao.yang,benoit.geller,tarak.arbi@ensta-paristech.fr

ABSTRACT

In this paper, an original physical layer design of the IEEE 802.15.6 narrowband receiver is proposed, including frame synchronization, timing synchronization, and carrier frequency synchronization. This proposed single-carrier system can be incorporated into a conventional multi-carrier system of the IEEE 802.11 transceiver by reusing its hardware resource. Simulation results show that the performances of the proposed system approach closely to the theoretical performances.

Index Terms—Wireless Body-Area Network (WBAN), Internet of Things (IoT), Physical Layer Design, IEEE 802.15.6, Frame Synchronization, Timing Synchronization, Carrier Frequency Synchronization, 802.11.

1. INTRODUCTION

The IEEE 802.15.6 standard [1] is a short-range (within 3 m range), low power, wireless communication standard in close proximity to body area to offer reliable real-time medical and non-medical services. Medical WBANs (Wireless Body Area Network) consist of implant devices and wearable medical systems to measure the health status. Non-medical WBAN includes wearable consumer electronics and entertainment devices. Differently from the UWB mode of the IEEE 802.15.6 standard targeting non-medical applications, the narrowband mode standard [2] particularly aims at becoming an IoT (internet of things) standard for the future healthcare and medical industries. Therefore, this paper focuses on the narrowband mode.

Over the 2.4-GHz ISM band, several important wireless communication standards coexist, including IEEE 802.11a/b/g/n (WiFi) [3], IEEE 802.15.1 (Bluetooth) [4], IEEE 802.15.4 (ZigBee) [5], and IEEE 802.15.6 (Wireless Body-Area Network, WBAN) standards. Among these standards, the IEEE 802.11a/b/g/n standard is the most popular wireless communication standard. For the WBAN standard, it would be extremely attractive to have the same coverage as the WiFi standard. Therefore, differently from the works in [6]-[12], this paper intends at designing a single-carrier receiver for the IEEE 802.15.6 narrowband

mode by exploiting multi-carrier signal processing algorithms, such as used in the 802.11a/b/g/n standard.

This paper is organized as follows. The physical layer specifications of the IEEE 802.15.6 narrowband signal are recalled in section 2. The WiFi compatible designs for the physical layer of IEEE 802.15.6 standard are detailed in section 3. The performances of the proposal are displayed in section 4. Conclusion is made at the end of this paper.

2. PHYSICAL LAYER SPECIFICATION OF IEEE 802.15.6 NARROWBAND SIGNAL

The IEEE 802.15.6 physical layer frame structure is shown in Fig.1. The physical layer consists of three parts, *i.e.*, the Physical Layer Convergence Protocol (PLCP) preamble, the PLCP header and the physical layer service data unit (PSDU). The latter two parts together are called Physical layer Protocol Data Unit (PPDU).
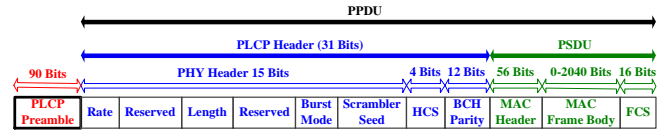

Fig.1. IEEE 802.15.6 WBAN physical layer frame structure

The first part is the PLCP preamble. It serves as a known training sequence for baseband processing functions, such as frame synchronization (or packet detection), timing synchronization, frequency synchronization. For the narrowband mode, two types of PLCP preambles are defined in order to reduce false alarms coming from the networks operating on adjacent channels. Each preamble is defined by concatenating a 63-bit M-sequence with the following 27-bit extension sequence 010101010101101101101101101. Since the preamble bit sequence is $\pi/2$-DBPSK modulated, the preamble contains 90 complex-valued symbols.

The second part of the frame is the PLCP header and is also the first component of the PPDU. The 31-bit-PLCP header includes the most important physical layer coding and modulation parameters, a header check sequence (HCS) and BCH parity bits. Since this part is also $\pi/2$-DBPSK

modulated, the PLCP header contains 31 complex-valued symbols.

The last part of the frame is the PSDU is also the last part of the PPDU. This part contains the MAC header, a MAC frame body which contains the useful information and a frame check sequence (FCS). The PSDU is then encoded and spread/interleaved before being scrambled. For the narrowband mode, the binary sequence in the PSDU is mapped onto one of the three rotated and differentially encoded constellations: $\pi/2$-DBPSK, $\pi/4$-DQPSK or $\pi/8$-D8PSK.

Table I. $\pi/2$-DBPSK

$b(k)$	φ_k
0	$\pi/2$
1	$-\pi/2$

Table II. $\pi/4$-DQPSK

$b(2k)$, $b(2k+1)$	φ_k
0, 0	$\pi/4$
0, 1	$3\pi/4$
1, 0	$7\pi/4$
1, 1	$5\pi/4$

Table III. $\pi/8$-D8PSK

$b(2k)$, $b(2k+1)$, $b(3k+2)$	φ_k
0, 0, 0	$\pi/8$
0, 0, 1	$3\pi/8$
0, 1, 0	$7\pi/8$
0, 1, 1	$5\pi/8$
1, 0, 0	$15\pi/8$
1, 0, 1	$13\pi/8$
1, 1, 0	$9\pi/8$
1, 1, 1	$11\pi/8$

For any of the previous differentially encoded constellations, the binary bit stream $b(n)$, $n = 0, 1, \ldots, N-1$ is mapped onto a corresponding complex-valued sequence $s(k)$, $k = 0, 1, \ldots, (N/\log_2(M))-1$ as shown as below:

$$s(k) = s(k-1)\exp(j\varphi_k), \quad (1)$$

where M is the constellation order, $s(-1) = \exp(j\pi/2)$ is the reference for the first symbol of the preamble and the phase transitions between symbols φ_k are given in Table I, Table II or Table III for $\pi/2$-DBPSK, $\pi/4$-DQPSK or $\pi/8$-D8PSK, respectively.

Due to the short communication range, as well as the low symbol rate, the communication channel can be treated as a flat-fading and slow-varying channel. Therefore, the received observation signal can be modeled as:

$$r(t) = h\sum_n s_n u(t - nT_{symb}) + w(t), \quad (2)$$

where $u(t)$ is the conventional square-root raised cosine (SRRC) pulse shaping filter, h is the slow-varying flat-fading channel attenuation and is treated as a constant within a packet reception period.

Based on (2), the received baseband processing should include frame synchronization, carrier frequency synchronization, and timing synchronization before performing differential DMPSK symbol detection. It should be mentioned that carrier phase synchronization is not performed thanks to the differential detection applied for demapping DMPSK symbols.

3. PHYSICAL LAYER DESIGN

In this section, the various baseband signal processing blocks – frame synchronization, carrier frequency synchronization and timing synchronization are detailed.

3.1. Frame synchronization

Since the IEEE 802.15.6 system is a packet-based transmission system, locating the start of frame (SOF) should be the first task to be established before any other baseband processing. Therefore, the frame synchronization should tolerate various front-end impairments such as sampling clock timing offset, carrier frequency offset, and additive noise.

In order to perform robust frame synchronization over the received samples with sampling rate $f_{samp} = 2f_{symb}$, the following time-domain correlation algorithm is proposed:

$$\hat{n}_{\text{SOF}} =$$

$$\arg\left\{\max_n\left\{\sum_{l=1}^{L}\left\|\sum_{p=0}^{89-l} r\left(n + p + l\frac{T_{symb}}{T_{samp}}\right)r^*(n+p)\prod_{q=0}^{l}\exp\left\{-j\tilde{\varphi}_{p+q}\right\}\right\|\right\}\right\}, \quad (3)$$

where $\hat{n}_{\text{SOF}}$ is the estimated start of frame (SOF), $r(n)$ is the received oversampled observation at time instante n, $T_{symb} = 1/f_{symb}$ is the symbol time interval, $T_{samp} = 1/f_{samp}$ is the sampling time interval, $\tilde{\varphi}_n$ is the n-th phase transition between the successive DMPSK symbols $s(n)$ and $s(n-1)$. Two points should be noted: First, the differential correlation term $r\left(n + l\frac{T_{symb}}{T_{samp}}\right)r^*(n)$ reduces the impact of the carrier frequency offset without having been established yet. Second, the index l indicates that the correlation is not only performed between consecutive symbol-time spaced samples, it is also performed between with several symbol-time spaced samples. This improves the robustness of the frame synchronization.

In the proposed frame synchronization, $L=2$ is enough to locate SOF with a carrier frequency offset $f_{CFO} = 0.1 f_{symb}$ and a signal-to-noise ratio SNR = -1 dB.

3.2. Carrier frequency synchronization

Proceeded the frame synchronization, the carrier frequency synchronization is the second to be established. It has huge impact over the timing synchronization and the symbol detection.

Similarly to a conventional OFDM system, the carrier frequency synchronization consists of a coarse CFO (carrier frequency offset) synchronization step and a fine CFO synchronization step.

The coarse CFO synchronization is performed over the received oversampled observations as follows:

1) Transform every N_{FFT}^{CFO} oversampled time-domain preamble observations into the frequency domain by FFT. The corresponding frequency-domain preamble observations are designated as $\tilde{R}(k)$, $k = 0, 1, \ldots, N_{FFT}^{CFO} - 1$;

2) Transform the corresponding $N_{FFT}^{CFO}/2$ time-domain preamble into the frequency domain by FFT. The corresponding frequency-domain preamble observations are designated as $\tilde{P}(k)$, $k = 0, 1, \ldots, N_{FFT}^{CFO}/2 - 1$;

3) Perform shift correlation and locate the maximum correlation between the two frequency-domain sequences as:

$$\hat{n}_{coarse}^{CFO} =$$

$$\arg\left\{\max_{n}\left\{\left\|\begin{array}{l}\sum_{p=0}^{N_{FFT}^{CFO}/4-1}\tilde{R}\left((p+n)\bmod N_{FFT}^{CFO}\right)\tilde{P}^*(p) \\ +\sum_{p=N_{FFT}^{CFO}/4}^{N_{FFT}^{CFO}/2-1}\tilde{R}\left(\left(p+\frac{N_{FFT}^{CFO}}{2}+n\right)\bmod N_{FFT}^{CFO}\right)\tilde{P}^*(p)\end{array}\right\|\right\}\right\},$$
(4)

where $\bmod N_{FFT}^{CFO}$ means a module N_{FFT}^{CFO} operation.

The estimated CFO $\tilde{f}_{coarse}^{CFO}$ is then equal to:

$$\hat{f}_{coarse}^{CFO} = \hat{n}_{coarse}^{CFO}\frac{f_{samp}}{N_{FFT}^{CFO}}$$
(5)

4) Compensate the CFO $\tilde{f}_{coarse}^{CFO}$. ∎

It can be noted that the estimated CFO by the coarse CFO estimation algorithm has a precision of f_{samp}/N_{FFT}^{CFO}. In this algorithm, the FFT size N_{FFT}^{CFO} determines the precision: the larger the value N_{FFT}^{CFO}, the finer the precision of the estimator.

In the proposed coarse CFO estimator, N_{FFT}^{CFO} = 128 is used corresponding to 128 preamble samples and corresponding to 64 preamble symbols due to $f_{samp} = 2 f_{symb}$. Therefore, for every packet containing 90 preamble symbols, there are two

partially correlated CFO estimates $\tilde{f}_{coarse}^{CFO}$. In the proposed system, with N_{FFT}^{CFO} = 128, the residual CFO can always be suppressed within the order of f_{samp}/N_{FFT}^{CFO} for an initial carrier frequency offset $f_{CFO} = 0.1 f_{symb}$ and a signal-to-noise ratio SNR = -1 dB.

After the coarse CFO compensation, a fine CFO synchronization is performed over the coarse CFO compensated time-domain preamble symbols $\tilde{r}(n)$ as follows:

$$\hat{f}_{fine}^{CFO} = \frac{1}{2\pi L T_{symb}}$$
$$\cdot\tan^{-1}\left\{\sum_{l=1}^{L}\frac{1}{(90-l)l}\sum_{p=0}^{89-l}\tilde{r}(p+l)\tilde{r}^*(p)\prod_{q=0}^{l}\exp\left\{-j\tilde{\varphi}_{p+q}\right\}\right\}.$$
(6)

In order to simply the system complexity, the fine CFO is estimated as follows:

$$\hat{f}_{fine}^{CFO} = \frac{1}{\pi T_{symb}}\cdot\tan^{-1}\left\{\hat{v}_{fine}^{CFO}\right\},$$
(7)

where $\hat{v}_{fine}^{CFO}$ is computed by using a one-tap IIR filter:

$$\hat{v}_{fine}^{CFO} = (1-\alpha)\hat{v}_{fine}^{CFO} + \alpha\frac{1}{l}\tilde{r}(p+l)\tilde{r}^*(p)\prod_{q=0}^{l}\exp\left\{-j\tilde{\varphi}_{p+q}\right\}.$$
(8)

In the proposed fine CFO estimator, the values $L=2$ and $\alpha = 0.01$ are used.

3.3. Timing synchronization

In the proposed design, the timing synchronization is the last task to be achieved before the differential symbol detection. Its objective is to estimate the delay parameter τ in the signal $r(t-\tau)$, where one has

$$r(t-\tau) = h\sum_n s_n u\left(t-nT_{symb}-\tau\right)+w(t-\tau).$$
(9)

Differently from a conventional timing synchronization is generally composed of two blocks, namely the symbol interpolator and the timing error detector (TED), the proposed timing synchronizer intends to estimate the global channel impulse response $hu\left(t-nT_{symb}-\tau\right)$ and behaves more like a channel estimator. Therefore, the timing recovery involves two different blocks: channel estimator and channel equalizer.

The channel estimator aims at estimating the frequency-domain channel transfer function based on the CFO compensated oversampled observations and the known preamble symbols, on thus performs the following steps:

1) Transform every N_{FFT}^{TR} oversample time-domain preamble observations into the frequency domain by FFT. The corresponding frequency-domain CFO compensated preamble observations are designated as $\tilde{R}(k)$, $k = 0, 1, \ldots, N_{FFT}^{TR} - 1$;

2) Insert 1 zero for every preamble symbol in the time domain, and then transform the zero-inserted N_{FFT}^{TR} preamble symbols into the frequency domain by FFT.

The corresponding frequency-domain preamble pilots are designated as $\tilde{P}(k)$, $k = 0, 1, \ldots, N_{FFT}^{TR} - 1$;

3) Like for a conventional OFDM channel estimator, the channel transfer function can be estimated as $\hat{H}(k) = \tilde{R}(k)/\tilde{P}(k)$;

4) Linear interpolate the frequency-domain channel transfer responses between consecutive $\hat{H}(k)$ values. One has a new interpolated frequency-domain channel transfer function $\hat{H}_I(k)$ of length $2N_{FFT}^{TR}$. ∎

The channel equalizer then launches the overlap-save (OLS) method [13] to perform the frequency-domain equalization over the twice-oversampled samples as following:

1) Take the last N_{FFT}^{TR} oversampled observations from the previous OLS block;

2) Take the newly N_{FFT}^{TR} oversampled observations which need to be equalized;

3) Transfer the $2N_{FFT}^{TR}$ samples into the frequency domain which are then designated as $R(k)$;

4) Perform a linear equalization as $\hat{D}(k) = R(k)/\hat{H}_I(k)$;

5) Transform the equalized frequency-domain samples $\hat{D}(k)$ back into the time domain;

6) Output the last N_{FFT}^{TR} samples, among which, the first sample of every two samples is the timing recovered DMPSK symbol. ∎

In the proposed timing synchronizer, $N_{FFT}^{TR} = 64$ is used for the channel estimation.

4. SIMULATION RESULTS

In this section, the performance of the proposed system for $\pi/2$-DBPSK (see Fig.2), $\pi/4$-DQPSK (see Fig.3) and $\pi/8$-D8PSK (see Fig.4) is evaluated for two scenarios: one is the simulation with a random timing offset (RTO) $\tau \in \left[-T_{symb}/2, T_{symb}/2 \right)$ (see the curves indicated as "RTO Sim") and the other is with a RTO and a large CFO $f_{CFO} = 0.1 f_{symb}$ (see the curves indicated as "RTO + 10% CFO Sim"). In these simulations, all the baseband processing blocks (frame synchronization, carrier frequency synchronization and timing synchronization) are active and therefore the estimation errors exist. In order to be fairly compared with the corresponding theoretical performances for differential detected $\pi/2$-DBPSK, $\pi/4$-DQPSK and $\pi/8$-D8PSK signals, the simulated performances are evaluated without the use of the BCH decoder. Moreover, the theoretical performance (indicated as "Theory") represents the best performance over AWGN channel with differential detection method and serve as a reference performance [14].
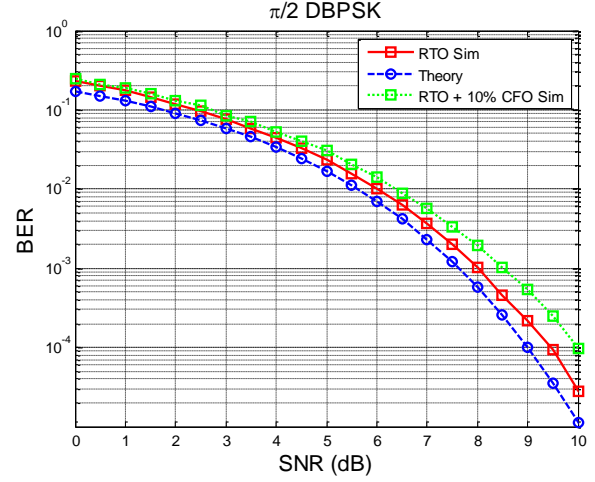

Fig.2. The simulation performance of the proposed system for a $\pi/2$-DBPSK signal.
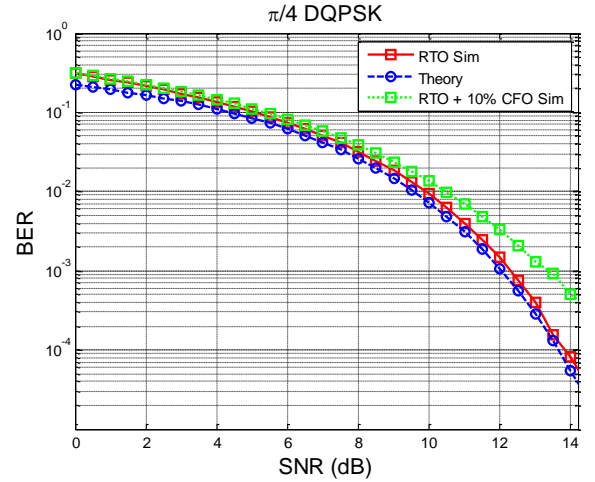

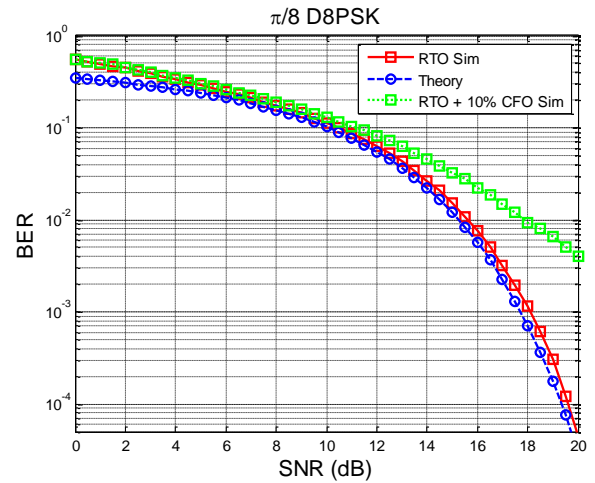Fig.3. The simulation performance of the proposed system for a $\pi/4$-DQPSK signal.

Fig.4. The simulation performance of the proposed system for a $\pi/8$-D8PSK signal.

It can be observed from Fig.2 to Fig.4 that the bit error rate (BER) curves follow closely the theoretical performance for

all the $\pi/2$-DBPSK, $\pi/4$-DQPSK and $\pi/8$-D8PSK signals with only RTO. As the CFO increases, the BER curves deviate from the corresponding theoretical curves as expected from the nature of the differential modulation. As the constellation order increases, the signal becomes more and more sensitive to the CFO.

5. CONCLUSION

In this paper, the design of physical layer algorithms for IEEE 802.15.6 narrowband receiver was presented. Differently from the conventional design for a single-carrier transceiver, the proposed signal processing algorithms can directly be applied to an OFDM based communication system such as WiFi [3]. Through numerical simulations, the proposed algorithms follow closely the corresponding theoretical performances over an AWGN channel with random timing errors. This indicates that the proposal introduces a negligible level of estimation error. This design is therefore attractive for the design of a multi-standard and multi-mode transceiver and can potentially push the IEEE 802.15.6 WBAN standard to more applications. In the future we aim at including in our multi-standard receiver a soft decoder [15]-[16] to both take fully advantage of a soft synchronization [17]-[18] and of a cross-layer design [19]-[23].

6. REFERENCES

[1] "IEEE Standard for Local and metropolitan area networks – Part 15.6: Wireless Body Area Networks," 2012.
[2] C. Lee, J. Kim, H. S. Lee and J. Kim, "Physical layer designs for WBAN systems in IEEE 802.15.6 proposals," in the proceedings of 9th International Symposium on Communications and Information Technology, 2009. ISCIT 2009. pp. 841-844, Icheon, 2009.
[3] "IEEE Standard for Local and metropolitan area networks – Part 11: Wireless LAN Medium Access Control (MAC) and Physical Layer (PHY) Specifications," 2012.
[4] "IEEE Standard for Local and metropolitan area networks – Part 15.1: Wireless Medium Access Control (MAC) and Physical Layer (PHY) Specifications for Wireless Personal Area Networks (WPANs)," 2005.
[5] "IEEE Standard for Local and metropolitan area networks – Part 15.4: Low-Rate Wireless Personal Area Networks (LR-WPANs)," 2011.
[6] B. Choi, B. Kim, S. Lee, K. Wang, Y. Kim and D. Chung, "Narrowband Physical Layer Design for WBAN System," in the proceedings of First International Conference on Pervasive Computing Signal Processing and Applications (PCSPA), 2010, pp. 154-157, Harbin, 2010.
[7] BoHeun Choi, ByungSoo Kim and SangSeol Lee, et al. "Narrowband Physical Layer design for WBAN system," in the proceedings of First International Conference on Pervasive Computing, Signal Processing and Applications (PCSPA), pp. 154-157, Sep. 2010.
[8] Mengyuan Chen, Jun Han, Dabin Fang, Yao Zou and Xiaoyang Zeng, "An Ultra Low-Power and Area-Efficient Baseband Processor for WBAN Transmitter," in the proceedings of Signal and Information Processing Association Annual Summit and Conference (APSIPA), 2013.
[9] Yunping Liang, Yu Zhou and Ye Lu, "The design and implementation of IEEE 802.15.6 Baseband on FPGA," in the proceedings of International Conference on Health Informatics, IFMBE Proceedings 42, Nov. 2013.
[10] P. Mathew, L. Augustine, D. Kushwaha, V. Desalphine and A. David Selvakumar, "Implementation of NB PHY transceiver of IEEE 802.15.6 WBAN on FPGA," in the proceedings of 2015 International Conference on VLSI Systems, Architecture, Technology and Applications (VLSI-SATA), pp. 1-6., Bangalore, 2015.
[11] P. Mathew, L. Augustine, D. Kushwaha, D. Vivian and D. Selvakumar, "Hardware implementation of NB PHY baseband transceiver for IEEE 802.15.6 WBAN," in the proceedings of 2014 International Conference on Medical Imaging, m-Health and Emerging Communication Systems (MedCom), pp. 64-71, Greater Noida, 2014.
[12] G. Devita et al., "A 5mW multi-standard Bluetooth LE/IEEE 802.15.6 SoC for WBAN applications," in the proceedings of European Solid State Circuits Conference (ESSCIRC), ESSCIRC 2014 - 40th, pp. 283-286, Venice Lido, 2014.
[13] Proakis, J. G., and Manolakis, D. K., Digital Signal Processing, 4th Edition., Pearson, 2007.
[14] Xiong, F., *Digital Modulation Techniques (Second Edition)*, Artech House, April, 2006.
[15] I. Diatta, D. De Geest, B. Geller, "Reed Solomon Turbo Codes for High Data Rate Transmission", Proceedings of IEEE VTC, pp. 1023-1027, Milan, May 2004.
[16] B. Geller, I. Diatta, J.P. Barbot, C. Vanstraceele, F. Rambeau, " Block Turbo Codes : From Architecture to Application", Proceedings of IEEE ISIT, Seattle, July 2006.
[17] J. Yang, B. Geller, and A. Wei, "Bayesian and Hybrid Cramer-Rao Bounds for QAM Dynamical Phase Estimation", Proceedings of IEEE ICASSP'09, Taipei, April 2009.
[18] J. Yang, B. Geller, C. Herzet, and J.M. Brossier,"Smoothing PLLs for QAM Dynamical Phase Estimation", Proceedings of IEEE ICC'09, Dresden, June 2009.
[19] L. Zhou, B. Geller, X. Wang, A Wei, B. Zheng, H.C. Chieh, "Multi-user video streaming over multiple heterogeneous wireless networks: a distributed, cross-layer design paradigm", Journal of Internet, vol. 10, no 1, 2009.
[20] L. Zhou, B. Zheng, J. Cui, B. Geller, A.Wei, S. Xu, "Cross-Layer Design for Flow Control in Cooperative Multi-Hop Wireless Networks", International Journal of Innovative Computing, Information and Control, vol. 5 no 2, Feb. 2009.
[21] L. Zhou, X. Wang, Y. Li, B. Zheng, B. Geller, "Optimal scheduling for Multiple Description Video Streams in Wireless Multi-Hop Networks", IEEE Communications letters, vol. 13,no.7, pp. 1-3, July 2009.
[22] L. Zhou, B. Geller, B. Zheng, J. Cui, " Cross-Layer Design for Scheduling in Cooperative VANETS", Proceedings of IEEE ITST,Lille, October 2009.
[23] L. Zhou, B. Geller, A. Wei, B. Zheng, J. Cui, S. Xu, "Cross-Layer Rate Allocation for Multimedia Applications in Pervasive Computing Environment", Proceedings of IEEE GLOBECOM 2008, New Orleans, Nov. 2008.